Fabrication Imperfection Analysis of Robust Decoupled 3-DoF Non-Resonant MEMS Gyroscope

Kashif Riaz, M. Umer Mian, Shafaat A. Bazaz

Abstract— This paper reports behavioral model simulations of a three degree of freedom (3DoF) non-resonant micromachined gyroscope in the presence of fabrication imperfections. Fabrication variations in beam lengths, beam widths, structure thickness, elastic modulus of material result elastic asymmetries in gyroscope motion which causes resonance frequency shifts, displacement amplitude variations and zero rate output. These variations are simulated using worst case fabrication tolerance ranges provided by fabrication foundry of gyroscope. Simulation results demonstrate robustness of our design in suppressing such asymmetries by utilizing decoupled sense and drive modes and independent suspension system for drive and sense modes.

Index Terms—Behavioral model, Decoupled, Degree-of-freedom (DoF), Fabrication imperfections, Micromachined gyroscope, Non-resonant, Robust

1 INTRODUCTION

Fabrication variations are unavoidable and restrict the performance of micromachined gyroscopes. Every fabrication step such as deposition, patterning, etching etc have some tolerances and contribute to imperfections in MEMS devices. This result in asymmetries and perturbations in the form of mechanical and electrostatic forces; effect the performance of gyroscope. Gyroscope performance can be improved by understanding their behavior in the presence of fabrication imperfections [1].

These fabrication imperfections affect geometry and material properties of micromachined gyroscope. Major variations are in beam lengths and widths, structure thickness, elastic modulus and residual stresses [2, 3]. Lateral over etching is another imperfection which effect all dimensions at same time as it has statistical distribution [4]. Due to lateral over etching, sometimes trenches may not be straight which result in different top and bottom dimensions of a beam [5].

Small imbalance and asymmetries in suspension system due to fabrication variations in MEMS gyroscope cause anisoelasticities in structure which results in dynamic cross coupling between drive and sense modes [6, 7]. Electrical and mechanical balancing methods are used to cancel these asymmetries but these methods are complex, costly, time consuming, difficult to implement on small scale and reduces parasitic effects to a certain amount [8-10]. Various devices have been reported employing mechanically decoupled drive and sense modes by using a unidirectional frame structure or independent suspension system for two modes. This will suppress coupled motion, drift and zero rate output at great extent [6, 7, 11-13].

- *Kashif Riaz, Faculty of Electronic Engineering, GIK Institute of Engineering Sciences and Technolog, Pakistan. E-mail: engrkashifrz@gmail.com*
- *M. Umer Mian, Faculty of Electronic Engineering, GIK Institute of Engineering Sciences and Technolog, Pakistan. E-mail: umermian@gmail.com.*
- *Shafaat A. Bazaz, Dean, Department of Computer Sciences, CASE, Pakistan.*

Most traditional modeling and simulation tools mainly focus on the structural behavior without considering the device fabrication processes [14, 15]. Previously, fabrication imperfections effects in micromachined gyroscopes is investigated through theoretical probabilistic and deterministic approaches such as Monte-Carlo method and robust optimization approximation [1, 2, 4, 16-18] and developing theoretical models from the lumped-mass-spring models [14, 15]. These methods have limitations in analyzing the asymmetric defects and imperfections and assume many approximations which result errors in performance estimation. It is difficult to differentiate these errors from those caused by fabrication imperfections. Bo Lv, Gyimesi, Chiou and other used Finite Element Method (FEM) based simulations [5, 14, 19] to address the fabrication imperfections in micromachined devices. Modeling and simulations through finite element analysis (FEA) tools are time consuming and computational time is one of the major disadvantages of FEA. Iyer and Mukherjee used time efficient behavioral modeling approach to simulate fabrication imperfections through NODAS [2]. 2D models can be precisely solved but it is difficult to build 3D models through NODAS.

To overcome these problems, we have used behavioral modeling technique in CoventorWare [20] to simulate the performance of 3DoF non-resonant micromachined gyroscope in the presence of fabrication imperfections. A behavioral modeling and simulation tool at system level performs simulation based on the behavior of device as expressed by reduced order modeling. Worst case tolerances in lengths, widths, thickness and young modulus of devices provided by fabrication foundry of gyroscope are used to simulate its performance. Simulation results clearly indicate the advantage of utilizing mechanically decoupled drive and sense modes through unidirectional frame structure and independent suspension system for drive and sense modes in our 3DoF micromachined gyroscope design. The micromachined gyroscope has been fabricated using standard micromachined MetalMUMPS process using Nickel as structural layer [21]. Using fabricated prototype,

International Journal of Scientific & Engineering Research Volume 4, Issue 8, August-2013
ISSN 2229-5518

different measurements of dimensions are taken using scanning electron microscopy. These fabricated dimensions are different from design values due to imperfections introduce by fabrication process. Experimental characterization results show that device is operational due to advantage of our design even after fabrication imperfection.

2 3-DoF Non-Resonant Micromachined Gyroscope Model

The 3-DoF micromachined gyroscope consists of two interconnected masses m_1 and m_2 which are mechanically decoupled using decoupling frame of mass m_f as shown in figure 1. figure 2 shows the lumped mass-spring-damper model of proposed 3-DoF micromachined gyroscope with its suspension system that anchors the outer mass m_1 with substrate comprised of four double-folded beam flexures configuration with equivalent spring constant k_{1x} and restricted the motion of mass m_1 in drive direction (x-axis) only. Decoupling frame is connected to the mass m_1 via four double-folded beam flexures configuration with equivalent spring constant k_{2x} which can move only in drive direction.

Thus dynamic amplification of oscillations in drive mode of the sense mass m_2 is achieved by designing this active-passive mass configuration.

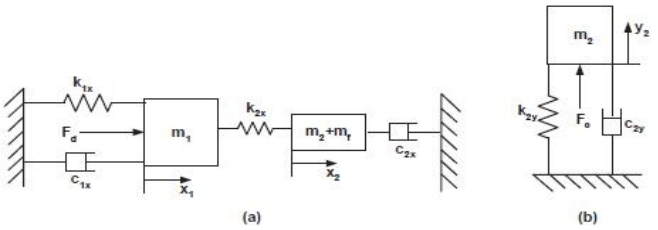

Fig. 2. Lumped mass-spring-damper model of 3-DoF micromachined Gyroscope (a) 2-DoF drive-mode oscillator (b) 1-DoF sense-mode oscillator.

Sensitivity is improved by utilizing resonance only in the sense mode of 3-DoF design concept while maintaining its robust operational characteristics. The 2-DoF drive-mode oscillator has two resonant peaks with a flat operational region between them. This region defines the operational frequency region of the micromachined gyroscope. In this flat operational region, response amplitude is less sensitive to fabrication and environmental variations. High robustness and stability is achieved by designing the 1-DoF sense-mode oscillator so that its resonant peak overlaps the flat operational region of the 2-DoF drive-mode oscillator.

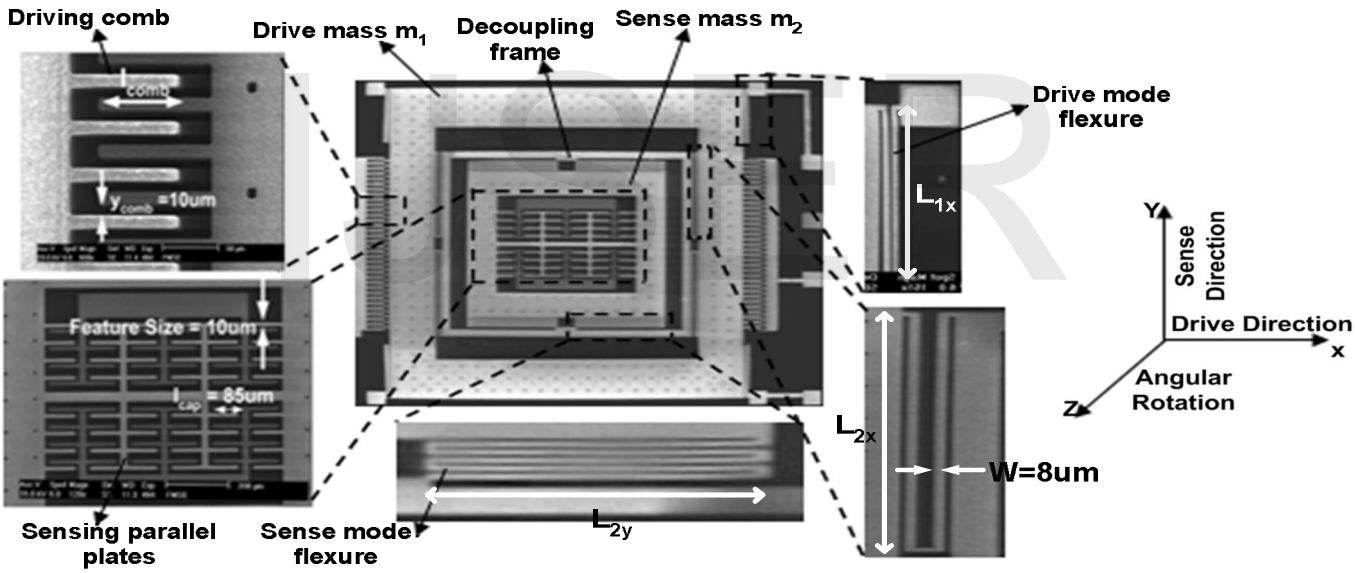

Fig. 1. SEM image 3DoF non-resonant micromachined gyroscope with suspension system.

The mass m_1 is electrostatically actuated using comb drives at resonant frequency of the mass m_2. When rotation is provided along z-axis, the mass m_2 will oscillate at its resonance frequency in response to coriolis force in sense direction (y-axis) due to four five-folded beam flexures configuration with equivalent spring constant k_{2y} which allow movement in the sense direction only. The amplitude of coriolis force is proportional to angular rate so response of the mass m_2 gives information about angular rate which is sensed through differential change in capacitance through parallel plates.

The overall gyroscope dynamical system consists of 2-DoF drive-mode oscillator and 1-DoF sense-mode oscillator. The mass m_2+m_f form the passive mass of 2-DoF drive-mode oscillator and acts as the vibration absorber of the active mass m_1.

The overall stiffnesses k_{1x}, k_{2x} and k_{2y} of the suspension system shown in Figure 2 are derived as [23]:

$$k_{1x} = \frac{4}{2}\left(\frac{1}{2}\frac{3EI}{(\frac{L_{1x}}{2})^3}\right) = \frac{2Etw^3}{L_{1x}^3} \quad (1)$$

$$k_{2x} = \frac{4}{2}\left(\frac{1}{2}\frac{3EI}{(\frac{L_{2x}}{2})^3}\right) = \frac{2Etw^3}{L_{2x}^3} \quad (2)$$

International Journal of Scientific & Engineering Research Volume 4, Issue 8, August-2013
ISSN 2229-5518

$$k_{2y} = \frac{4}{5}\left(\frac{1}{2}\frac{3EI}{(\frac{L_{2y}}{2})^3}\right) = \frac{4Etw^3}{5L_{2y}^3} \quad (3)$$

where E is the Young's Modulus of structural layer Nickel and it was assumed to be 214GPa, $I = tw^3/12$ is the second moment of inertia of the beam cross section, t is the beam thickness and w is the beam width.

The location of the two expected resonance peaks in the the drive-mode frequency response f_{x-n1} and f_{x-n2} are calculated by using the relations [6]:

$$f_{x-n_1} = \sqrt{\frac{1}{2}(1+\mu_x+\frac{1}{\lambda_x^2}-\sqrt{(1+\mu_x+\frac{1}{\lambda_x^2})^2-\frac{4}{\lambda_x^2}})}\,\omega_{2x} \quad (4)$$

$$f_{x-n_2} = \sqrt{\frac{1}{2}(1+\mu_x+\frac{1}{\lambda_x^2}+\sqrt{(1+\mu_x+\frac{1}{\lambda_x^2})^2-\frac{4}{\lambda_x^2}})}\,\omega_{2x} \quad (5)$$

Different design parameters of gyroscope are given in Table 1. The proposed design has been prototyped using standard surface micromachining MetalMUMPs process [21] which has structural layer thickness of 20µm. MEMSPro has been use for the designing of mask layouts, design rule checks and process simulations for MetalMUMPs. The major process steps of MetalMumps are shown in figure 3. Deatiled analysis on design is given in [22].

3 Behavioral Modeling and Frequency Analysis of Design Concept

The designed micromachined gyroscope performance is carried out through behavioral modeling using Coventorware Architect Module by modeling complete fabrication process and gyroscope design. This technique is computationally faster than FEM [20]. The main components used for the behaveioral modeling of design are rigid plate, comb-drive, beam and extracted slide and squeeze film damping macro-models to incorporate the effect of damping. Figure 4 shows the complete schematic model of the micromachined gyroscope behavioral model with the illustration of the physical geometry represented by the schematic components. In schematic, mechanical wires are a bundle of 6 individual wires containing three translational and three rotational degrees of freedom. Knot (figure 4) can be seen as the physical connection point between two or more mechanical elements [20].

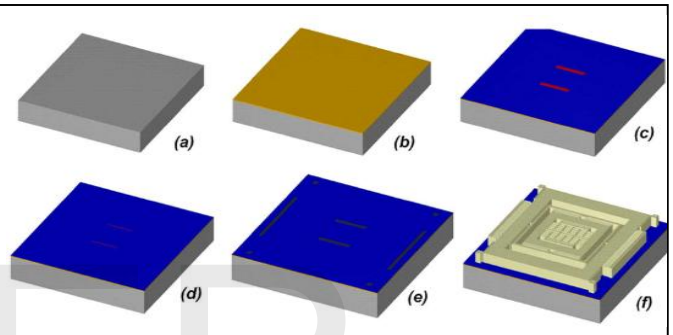

Fig. 3. Process flow for the fabrication of micromachined gyroscope using MetalMUMPs in MEMSPro (a) N-type<100>silicon wafer, (b) 2µm thick isolation oxide layer, (c) patterning of 0.35µm thick silicon nitride layers, (d) patterning of 0.7µm thick Polysilicon layer, (e) patterning of anchor metal layer, and (f) patterning of 20µm electroplated structural layer of Ni and trench etch in the substrate.

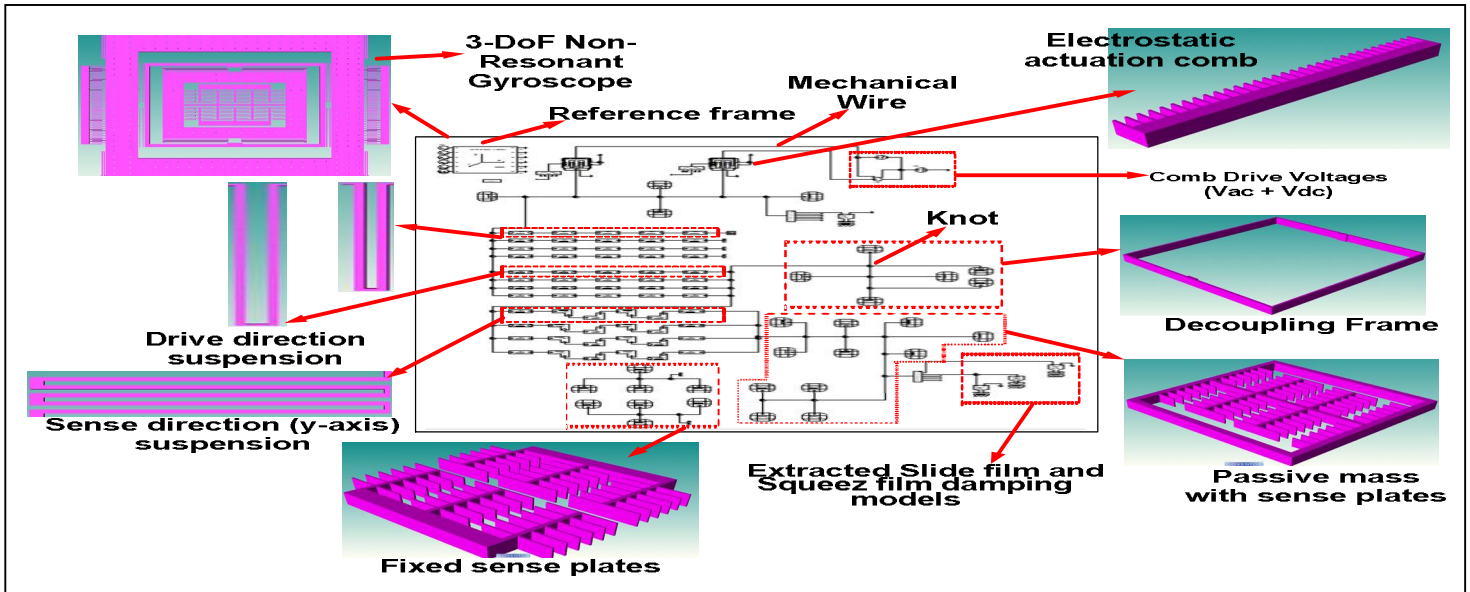

Fig. 4. Behavioral model Schematic of the proposed microgyroscope design with illustration of the physical geometry.

International Journal of Scientific & Engineering Research Volume 4, Issue 8, August-2013
ISSN 2229-5518

TABLE 1
DESIGN PARAMETERS OF 3-DOF MICROMACHINED GYROSCOPE.

Symbol	Quantity	Desined Values
m_1	Mass	3.86×10^{-7}kg
m_2+m_f	Mass	1.826×10^{-7}kg
L_{1x}	Length of outer flexure beam	410μm
L_{2x}	Length of decoupling frame flexure beam	650μm
L_{2y}	Length of inner flexure beam	502μm
w	Width of flexure beams	8μm
h	Height of flexure beams	20μm
t	thickness of flexure beams	8μm
k_{1x}	Flexure system	63.59N / m
k_{2x}	Flexure system	15.96N / m
k_{2y}	Flexure system	13.86N / m
ω_{1x}	Resonant frequency of the isolated active mass-spring system	2.043kHz
ω_{2x}	Resonant frequency of the isolated passive mass-spring system	1.490kHz
λ_x	Frequency ratio	0.7296
μ_x	Mass ratio	0.47
$f_{x\text{-}n1}$	First resonant peak in the the drive mode frequency response	1.25kHz
$f_{x\text{-}n2}$	Second resonant peak in the the drive mode frequency response	2.42kHz

To determine the device frequency characteristics, frequency analysis is carried out at 100 V_{dc} and 60 V_{ac} using developed behavioral model of gyroscope design at atmospheric pressure. Frequency analysis is carried out by varying the frequency from 1 Hz to 5 kHz. Figure 5(a) show that two resonance frequencies for the 2-DoF drive mode oscillator are located at 1.046 kHz and 2.042 kHz with a flat region of ~1 kHz between them. This region defines the operational frequency region of the microgyroscope where response amplitude is less sensitive to parameter variation. The sense mode frequency of 1.407 kHz is located inside the drive mode flat region as shown in figure 5(b), allowing the gyroscope to achieve high robustness and stability. Large oscillation amplitude of the sense element is achieved as shown in figure 5(a) which will increase output gain of gyroscope for higher sensitivity.

4 FABRICATION IMPERFECTION ANALYSIS

In surface micromachined gyroscopes, thin film deposition process determines the thickness of the structural layer including its micro-suspension elements, whereas etching process affects its width. Lateral over-etching often causes variation in the width and cross-section of the suspension beams and deposition conditions vary the elastic modulus of material. These unavoidable fabrication variations in suspension system and masses cause asymmetries in micromachined gyroscope response which result in resonant frequency shifts, displacement amplitudes variation and zero rate output. So simulation of micromachined designs in the presence of fabrication imperfections is necessary to improve the performance and to predict that either device will be operational in worst fabrication tolerance case or not.

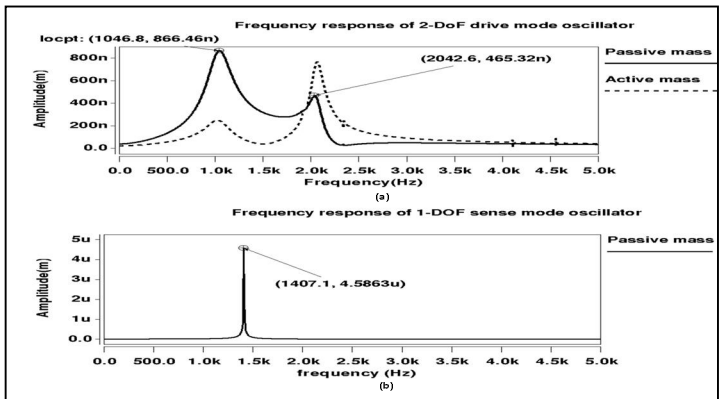

Fig. 5. Frequency response of 3DoF gyroscope (a) 2-DoF drive mode oscillator (b) 1-DoF sense mode oscillator.

Fabrication tolerances in MetalMUMPS process for worst case are provided by fabrication foundries and are listed in Table 2. These tolerance ranges are used to simulate the performance of gyroscope through behavioral modeling in the following section.

TABLE 2
WORST CASE FABRICATION TOLERANCES IN WIDTH, THICKNESS, AND YOUNG MODULUS OF STRUCTURAL LAYER NICKEL [21].

Width(μm)		
Minimum	Nominal	Maximum
7.5	8	8.5
Thickness(μm)		
Minimum	Nominal	Maximum
17	20	23
Young Modulus (GPa)		
Minimum	Nominal	Maximum
158	180	202

4.1 Width Variation Effects

In this section, the performance of design is analyzed with absolute tolerances in widths of beam and masses causing asymmetries in gyroscope. Absolute tolerances for width in MetalMUMPs process in worst case is ±0.5μm as given in Table 2. We have simulated the affect of imperfections due to width variation in flexures attached with mass m_1. Drive mode frequency analysis show that as the flexure width decreases, resonance frequencies and displacement amplitudes also decreases and vice versa but the operational bandwidth remain approximately constant as shown in figure 6(a). It can be ob-

International Journal of Scientific & Engineering Research Volume 4, Issue 8, August-2013
ISSN 2229-5518

served that the proposed design is robust to variations in spring widths, as there is negligible change in gain in the flat operational region and sense mode response still overlap the flat operational region.

Figure 6(b) clearly indicates that variation in outer beam width have no affect on sense mode frequency response and displacement amplitude. Decoupling frame and independent suspension for drive and sense mode make sensing differential capacitors sensitive only to the movement of mass m_2 in y-axis due to coriolis force.

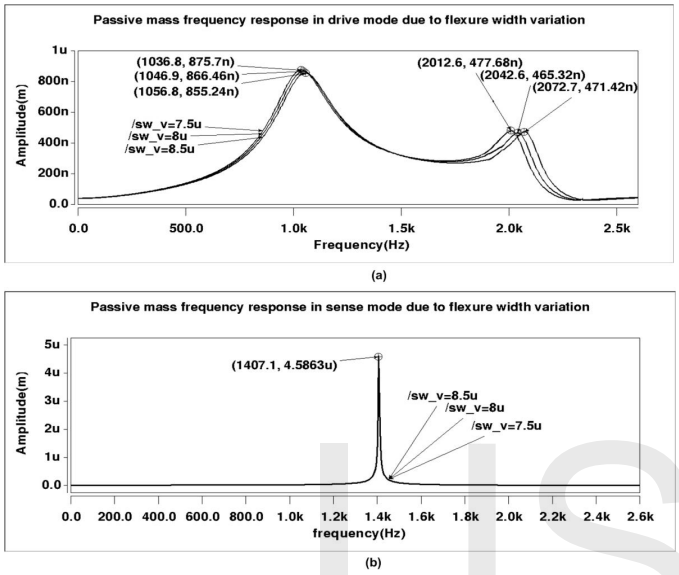

Fig. 6. Frequency response by varying outer flexure width (a) passive mass drive mode response (b) passive mass sense mode response.

Similarly, we have investigated the effect of width variation i.e. 7.5 µm to 8.5 µm in flexures attaching decoupling frame and drive mass m_1. The drive mode resonance frequencies and amplitudes have changed but gain in flat operational region has negligible change as shown in figure 7(a). This flexure width variation has no effect on sense mode frequency response as shown in figure 7(b) and has no effect on sense differential capacitance due to our design advantages.

To investigate the behavior of device due to width variations of inner flexures connected with sense mass m_2, widths of all four five-folded beam flexures are varied in fabrication tolerance range i.e. 7.5 µm to 8.5 µm and frequency analysis is carried out. Displacement amplitude and resonance frequency of passive mass in sense mode changes with the variation in inner flexures width as shown in figure 8(a). Inner flexure width variation has no effect on passive mass drive mode resonance frequencies and displacement amplitude due to our design approach. This shows that the dynamic cross coupling is suppressed from drive to sense mode and from sense to drive mode in our designed gyroscope.

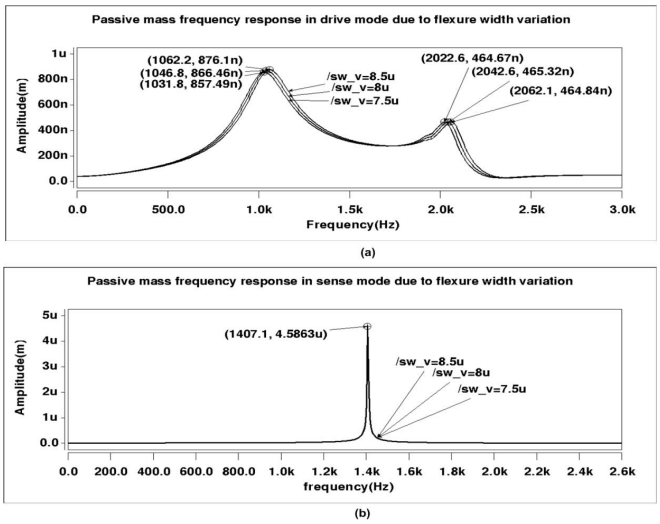

Fig. 7. Frequency response by varying middle flexure width (a) passive mass drive mode response (b) passive mass sense mode response.

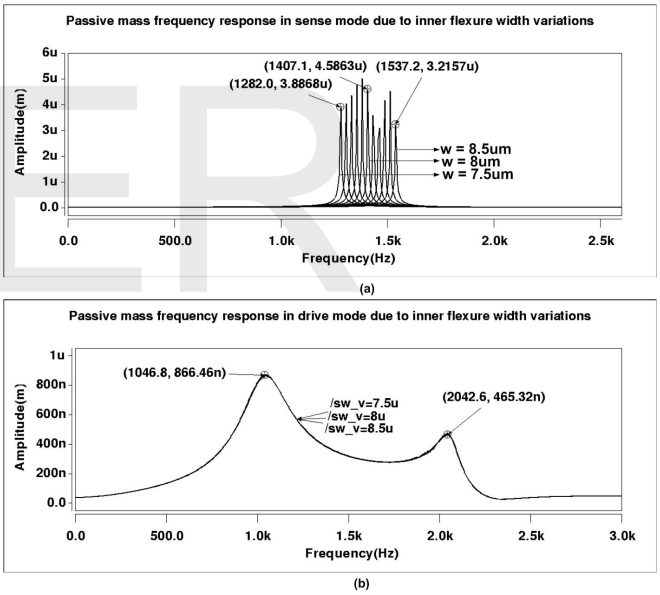

Fig. 8. Frequency response by varying all four inner flexures width (a) passive mass sense mode response (b) passive mass drive mode response.

From all above results we conclude following important results:

1. Variations in flexures width due to fabrication imperfections shift both the drive and sense mode resonance frequencies. Amplitudes of both drive and sense direction displacement have also been changed.

2. The operational bandwidth and gain in flat operational region remains almost constant even after worst case flexure width variations, making device robust against these structural variations.

International Journal of Scientific & Engineering Research Volume 4, Issue 8, August-2013
ISSN 2229-5518

3. Asymmetries have been introduced in gyroscope structure and also in its movement which may cause dynamic cross coupling in drive and sense modes. By utilization of decoupling frame and independent suspension system for drive and sense mode, such non-idealities and asymmetries can be suppressed without usage of feedback and tuning electronic circuitry as in our design.

4. Width variation of both masses have no significant effect on resonance frequencies and displacement amplitudes, as worst case tolerance in width is ±0.5µm which is very small as compare to area of masses.

4.2 Structure Thickness Variation Effects

Thin film deposition process determines the thickness of the structural layer which is Nickel in case of MetalMUMPS micromachining fabrication process. The nominal value for thickness is 20µm but worst case tolerance range is 17 – 23 µm as provided by fabrication foundry. Frequency analysis is carried out to investigate the effect of thickness variation in this range on response of gyroscope design as shown in Figure 7. The resonance frequencies and amplitudes increases with the increase of thickness and vice versa. In drive mode, there is only 0.28% shift at first resonance frequency and 0.1% frequency shift at second resonance frequency as shown in figure 9(a). A significant change of 10% in displacement amplitude is observed in drive mode clearly shown in figure 9(a).

In sense mode, resonance frequency approximately remains constant even at worst case tolerance of 3µm in thickness. But a significant variation in displacement amplitude in sense direction can be observed in figure 9(b), this change is about 12% at 3 µm thickness variations. But gain in flat operational region remains insensitive to thickness variation. This proves that the device will be functional in case of worst case thickness tolerance.

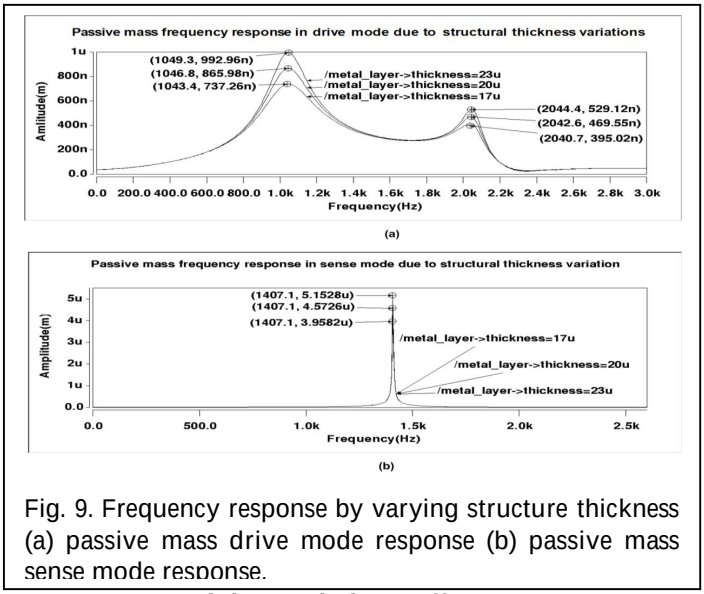

Fig. 9. Frequency response by varying structure thickness (a) passive mass drive mode response (b) passive mass sense mode response.

4.3 Young's Modulus Variations Effects

Thin film deposition process determines the thickness of the structural layer which Various values of young's modulus of Nickel film are in use by MetalMUMPS users. The young's modulus of electroplated nickel depends upon deposition and operating conditions and may vary from 158-202GPa as provided by fabrication foundry. It is necessary to investigate the effects of young's modulus variation on the performance of gyroscope. Frequency analysis is carried out by varying young's modulus of structural layer Nickel. Results indicate significant shifts in resonance frequencies and negligible variation in displacement amplitudes of masses. Resonance frequencies increases and amplitude decreases with the increase of young's modulus. There is approximately 6.2% shift in first resonance frequency and 6.6% shift in second resonant frequency in drive mode and variation of 2µm in displacement amplitudes is determined as shown in figure 10(a).

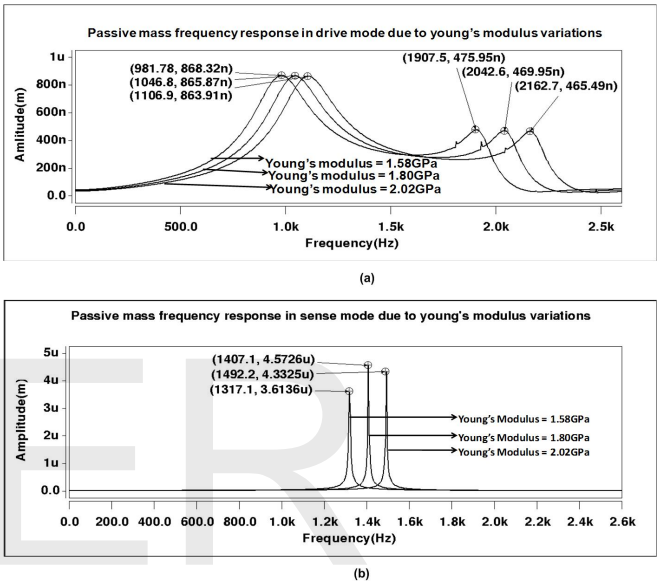

Fig. 10. Frequency response by varying young's modulus of Nickel (a) passive mass drive mode response (b) passive mass sense mode response.

Similarly, in sense mode there is 6.4% shift in resonance frequency and amplitude drop is less than 1µm as shown in figure 10(b). These results show that device will operate in flat operational region to achieve robustness and stability at worst case variation in young's modulus.

4.4 Environmental Variations Effects

Environmental variations such as pressure and temperature variations have significant effects on the performance of micromachined gyroscopes [6,24]. Damping which is directly proportional to operating pressure is the major energy dissipation mechanism in micromachined gyroscopes. The proposed device performance in the 2-DoF drive mode is analyzed by varying pressure from atmospheric pressure to vacuum through AC analysis. Simulation results show that the response is insensitive to pressure variations in the non-resonance flat operational region where device is designed to operate instead of resonance region (figure 11). For pressure variation from 100 militorrs to 500 militorrs, the device gain reduces to less than 1%, where same pressure variation results in more than 20% gain reduction in conventional micromachined gyroscopes [3].

International Journal of Scientific & Engineering Research Volume 4, Issue 8, August-2013
ISSN 2229-5518

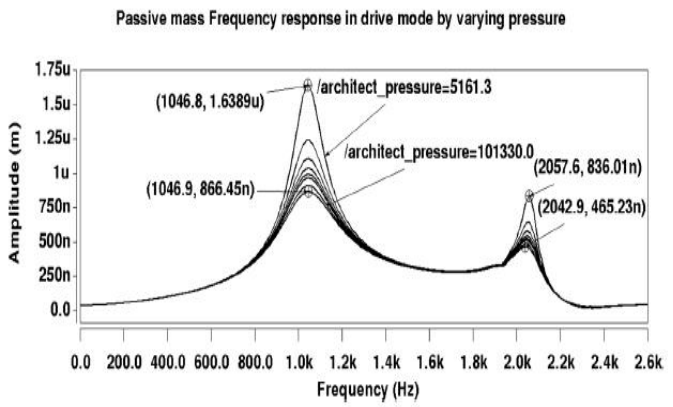

Fig. 11. Passive mass 2-DoF drive-mode response by varying pressure from 100 - 101325Pa.

Temperature variation also has significant effects on gain and resonant peak positions of micromachined gyroscope. Frequency response of the 2-DoF drive-mode oscillator shows that the maximum amplitude variation in the flat operational region is near 1% for temperature variation 250-300K as shown in figure 12. The gain drop at resonant peaks due to temperature variation which results in frequency shift is 2.2% for 50K variation in temperature. These simulation results show that gain in the flat operational region remain insensitive to environmental variations thus showing improved robustness to these variations.

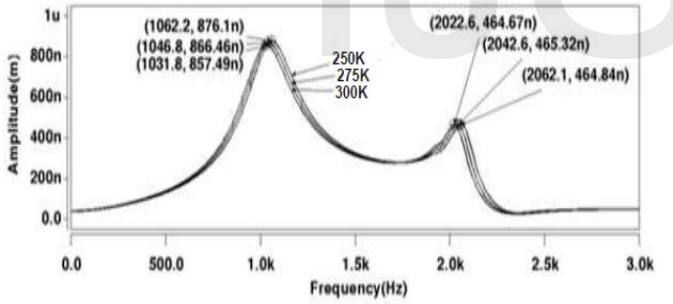

Fig. 12. Passive mass 2-DoF drive-mode response by varying temperature from 250 -300 K.

5 Fabricated Device Dimensions:

Dimensions of fabricated micromachined gyroscope have been measured using scanning electron microscopy such as lengths and widths of flexures and masses as shown in figure 13. These dimensions showed variations from design values as shown in table3.

Frequency analysis is carried out at 100V V_{dc}, 60V V_{ac} and at atmospheric pressure using new developed behavioral model with fabricated dimension values. Frequency analysis indicate 1st resonant frequency at 796.64 Hz with amplitude 890.05 nm and 2nd resonant frequency at 2199.3 Hz with amplitude 464.34 nm as shown in figure 14(a). The sense mode resonant frequency observed at 1807.4 Hz with amplitude 3.17 µm as shown in figure 14(b). These values indicated that fabrication imperfections have shifted the resonance frequencies of drive and sense modes and varied the displacement amplitudes. But by the utilization of independent suspension system for drive and sense modes and decoupled drive and sense mode, gyroscope suppressed asymmetries introduced by these fabrication imperfections and show safe operation in flat operation region. This eliminates the need of tuning and feedback electronics as the device is robust against structural variations.

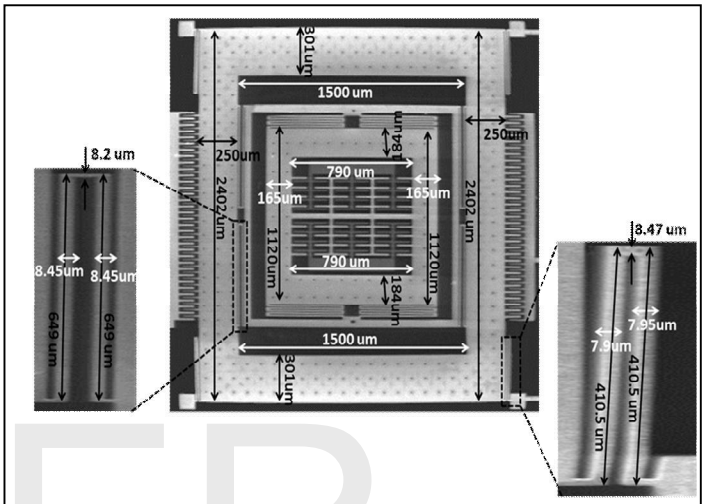

Fig. 13. Fabricated dimensions of 3DoF micromachined gyroscope prototype.

TABLE 3
DESIGNED AND FABRICATED DIMENSIONS VALUES OF 3DOF MICROMACHINED GYROSCOPE.

Parameters	Designed values	Fabricated values
k_{1x}	63.59 N / m	48.46 N / m
k_{2x}	15.96 N / m	17.18 N / m
k_{2y}	13.8 N / m	17.72 N / m
h	20µm	~20 µm

6 Experimental Characterization Results

The frequency response of 2-DoF drive mode oscillator and 1-DoF sense mode oscillator of the prototype 3-DoF micromachined gyroscope at atmospheric pressure was characterized at Nanoscale System Integration Group at Southampton University UK, using Polytec Microsystem analyzer, MSA-400 as shown in figure 15.

A peak-to-peak voltage signal is generated by an onboard signal generator from the MSA-400, which is then fed to the AC power amplifier for signal amplification. This amplified signal is applied to the electrostatic actuator. Finally, using the PMA-400 in-plane frequency response is extracted. For drive-mode characterization, two probes are used to apply +/- DC bias voltage on the fixed comb drives on either sides of the

International Journal of Scientific & Engineering Research Volume 4, Issue 8, August-2013
ISSN 2229-5518

microgyroscope whereas one probe is used to apply AC signal to the proof mass through the anchor. figure 16(a) and figure 16(b) present the frequency responses of the active mass m_1 and passive mass m_2. The first resonant frequency is observed at 754 Hz where the passive mass is observed to reach a displacement of 658 nm at 100 V_{dc} and 60 V_{ac} achieving a 3 times dynamic amplification of the active mass.

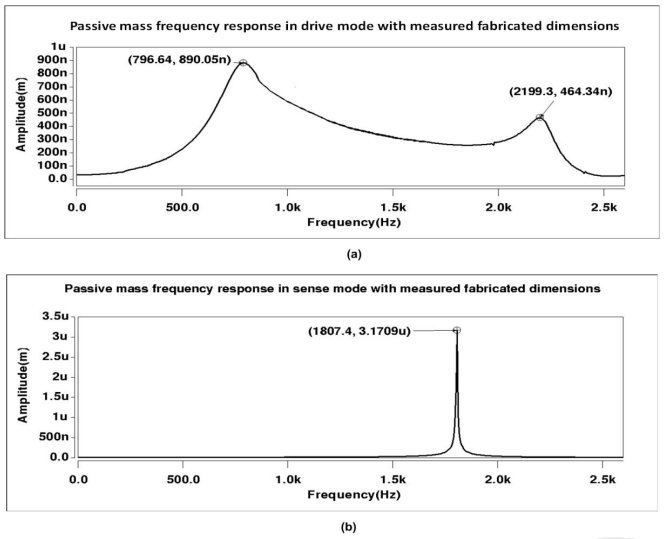

Fig. 14. Frequency response by using fabricated dimension (a) passive mass drive mode response (b) passive mass sense mode response.

Fig. 15. Experimental setup used to characterize the3DoF micromachined gyroscope

In drive mode frequency response, a flat region of 1.4 kHz is experimentally demonstrated. The two resonance peaks in the drive mode frequency response are observed at 754 Hz and 2.170 kHz instead of simulated values of 1.046 kHz and 2.042 kHz. At the second resonant frequency of 2.170 kHz, the passive mass is observed to reach a displacement of 460 nm at 100 V_{dc} and 60 V_{ac} achieving a 9 times dynamic amplification of the active mass having a displacement of 55nm.

Similar testing methodology is adopted to characterize sense-mode characterization. Two probes are used to apply +/- 60 VDC bias voltage on the fixed sides of the sensing parallel plate electrodes, whereas one probe is used to apply sinusoidal 45 VAC on the proof mass through the anchor. Figure 16(c) shows the frequency response of the 1-DoF sense mode oscillator. The location of the peak is observed at 1.868 kHz instead of simulated value 1.407 kHz. When the drive and sense mode frequency responses of the 3-DoF microgyroscope prototype are investigated together, a flat region of 1.4 kHz is overlapped by the sense-mode resonant frequency, defining the operation frequency region of the proposed device. These results experimentally demonstrate and verify the feasibility of the design concept. Table 4 summarizes the comparison of the simulation results of gyroscope with design parameters and test results.

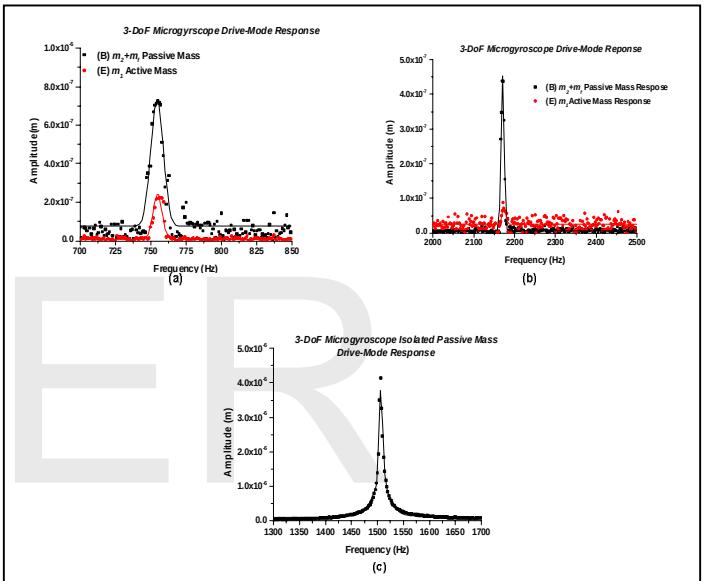

Fig. 16. 3-DoF micromachined gyroscope response (a) drive-mode response (first resonant frequency) (b) drive-mode response (second resonant frequency) (c) sense-mode response.

TABLE 4
COMPARISON OF THE SIMULATED AND TEST RESULTS FOR DRIVE AND SENSE MODES.

Parameters	Simulated Results		Experimental Results	
Drive mode first resonant frequency	796.64 Hz	890nm	754 Hz	658nm
Drive mode second resonant frequency	2.199kHz	464nm	2.170 kHz	460nm
Sense mode resonant frequency	1.8074 kHz	3.17 µm	1.868 kHz	4 µm

International Journal of Scientific & Engineering Research Volume 4, Issue 8, August-2013
ISSN 2229-5518

4 CONCLUSION

In this paper, we used behavioral modeling to simulate the fabrication imperfections effects in 3DoF micromachined gyroscope, as it is efficient in terms of time and memory requirements. Frequency analysis indicated resonance frequency shifts and displacement amplitude variations due to fabrication imperfections in width, thickness and young's modulus but designed bandwidth remain unchanged. Frequency analysis show the advantage of design approach in suppressing asymmetries caused by fabrication imperfections and makes the device functional even after worst case fabrication tolerances. Gyroscope design is robust to these structural fabrication variations due to the usage of decoupled drive and sense modes and independent suspension system for drive and sense modes. Experimental characterization results indicate the shifts in resonance frequencies and displacement amplitude variations as compare to simulation results but device is operational in flat operational region as predicted by fabrication imperfection simulations. Fabrication imperfection simulations prior to fabrication of prototype proved to be very effective to predict the functionality of gyroscope under fabrication imperfections.

REFERENCES

[1] A. Shkel, R. T. Howe, R. Horowitz, "Modeling and simulation of micromachined gyroscopes in the presence of imperfections", In: the International Conference on Modeling and Simulation of Microsystems, 1999, chapter 17, pp 605–608.

[2] Sitaramam Iyer and Tamal Mukherjee, "Simulation of manufacturing variations in a z-axis CMOS–MEMS gyroscope", In: International conference on modeling and simulation of microsystems, 2002, Vol. 1, pp 186–189.

[3] C. Acar and A. Shkel, "A Design Approach for Robustness Improvement of Rate Gyroscopes", In: the International Conference on Modeling and Simulation of Microsystems, 2001, Vol. 1, pp 80-83.

[4] Sung Kyu Ha, Hee-Moon Jeong and Juno Kim, "Robust design of a decoupled vibratory microgyroscope considering over-etching as a fabrication tolerance factor", JSME International Journal, Series A, Solid Mech Mat Eng, 2006, Vol. 49, pp 273–281.

[5] Bo Lv, Xuesong Liu, Zhenchuan Yang and Guizhen yan, "Simulation of a novel lateral axis micormachined gyroscope in the presence of fabrication imperfections", journal of Microsystem Technologies, 2008, Vol. 14, pp 711-718.

[6] Cenk Acar and Andrei M. Shkel, "Inherently robust micromachined gyroscopes with 2-Dof sense mode oscillator", Journal of Microelectromechanical System, 2006, Vol. 15, pp 380-387.

[7] Cenk Acar and Andrei M. Shkel, "An approach for increasing drive mode bandwidth of MEMS vibratory gyroscopes", Journal of Microelectromechanical System, 2005, Vol. 14, pp 520-528.

[8] Sungsu Park and Roberto Horowitz, "Adaptive control for the conventional mode of operation of MEMS Gyroscopes", Journal of Microelectromechanical System, 2003, Vol. 12, pp 101 - 108.

[9] P.B. Ljung, "Micromachined gyroscope with integrated electronics", Doctoral Thesis, U. C. Berkeley, 1997.

[10] X. Jiang, J. Seeger, M. Kraft and B.E. Boser, "A monolithic surface micromachined Z- axis gyroscope with digital output", IEEE 2000 Symposium on VLSI Circuits, Honolulu, HI, June 2000, pp.16-19.

[11] W. Geiger et al., "Decoupled microgyros and the design principle DAVED," IEEE Sensors J., pp. 170–173, 2001.

[12] Y. Mochida et al., "A micromachined vibrating rate gyroscope with independent beams for drive and detection modes", Sens. Actuators A. Phys., 2000, vol. 80, pp. 170–178.

[13] M. Niu et al., "Design and characteristics of two gimbals micro-gyroscopes fabricated with quasi-LIGA process," in Proc. Int. Conf. on Solid-State Sensor and Actuators, 1997, pp. 891-894.

[14] Miklos Gyimesi, Ilya Avdeev and Dale Ostergaard, "Finite Element Simulation of Microelectromechanical systems (MEMS) by Strongly Coupled Electromechanical Transducers", IEEE Transactions on Magnetics, Vol. 40, pp. 557–560, Mar. 2004.

[15] Changfti Zhang, Zhuangde Jiang, Dejiang Lu and Taian Ren, "3D MEMS Design Method via Solidworks", Proceedings of 1st IEEE International Conference on Nano / Micro Engineering and Molecular Systems, pp. 747-751, 2006.

[16] Luca Schenato, Wei-Chung Wu, Laurent El Ghaoui and Kristofer Pister, "Process Variation Analysis for MEMS Design", Proceedings of SPIE - The International Society for Optical Engineering, Vol. 4236, pp 272-279, 2001.

[17] Jeong Sam Han, Byung Man Kwak, "Robust optimal design of a vibratory microgyroscope considering fabrication errors", J. Micromech. Microeng., Vol. 11, pp 662–671, 2001.

[18] Hao Zhou, Hailin Tang, Wei Su and Xianxue Liu "Robust design of a MEMS gyroscope considering the worst-case tolerance", IEEE International Conference on Nano / Micro Engineered and molecular systems, Vol. 10, pp 1012–1016, 2010.

[19] A. Chiou, "Process window of micromachined gyroscopes subjected to vibrational frequencies", Sens Actuators A Phys., Vol. 125, pp 519–525, 2006.

[20] CoventorWare 2008, Using CoventorWare, www.coventor.com \coventorware.html

[21] A. Cowen, B. Dudley, E. Hill, M. Walters, R. Wood, S. Johnson, H. Wynands and B. Hardy, "MetalMUMPs Design Hand book (MEMSCap Inc. USA.)", www.memscap.com / mumps / documents / MetalMUMPs.DR.2.0.pdf

[22] Kashif Riaz, Shafaat A. Bazaz, M. Mubasher Saleem, and Rana I. Shakoor ,Y. Lai and M. M. Hasan, "Design, damping estimation and experimental characterization of decoupled 3-DoF robust MEMS gyroscope," Sensors and Actuators A: Physical, Vol. 172, Issue 2, December 2011, Pages 523–532.

[23] W.C. Young and R.G. Budynas, "Roarks Formulas for Stress and Strain," McGraw-Hill, New York, 2000, pp. 125-266.

[24] A.A. Trusov, A.R. Schoffeld, and A. Shkel, "Performance characterization of a new temperature-robust gain-bandwidth improved MEMS gyroscope operated in air," Sensors and Actuators A Physical, Vol. 155, 2009, pp. 16-22.